Fault detection and isolation of high temperature proton exchange membrane fuel cell stack under the influence of degradation

Jeppesen, Christian; Araya, Samuel Simon; Sahlin, Simon Lennart; Thomas, Sobi; Andreasen, Søren Juhl; Kær, Søren Knudsen

Published in:
Journal of Power Sources

DOI (link to publication from Publisher):
10.1016/j.jpowsour.2017.05.021

Publication date:
2017

Document Version
Early version, also known as pre-print

Fault Detection and Isolation of High Temperature Proton Exchange Membrane Fuel Cell Stack under the Influence of Degradation

Christian Jeppesen[a,*], Samuel Simon Araya[a], Simon Lennart Sahlin[a], Sobi Thomas[a], Søren Juhl Andreasen[b], Søren Knudsen Kær[a]

[a]*Department of Energy Technology, Aalborg University, Pontoppidanstræde 101, 9220 Aalborg Ø, Denmark*
[b]*Serenergy A/S, Lyngvej 8, 9000 Aalborg, Denmark*

Abstract

This study proposes a data-drive impedance-based methodology for fault detection and isolation of low and high cathode stoichiometry, high CO concentration in the anode gas, high methanol vapour concentrations in the anode gas and low anode stoichiometry, for high temperature PEM fuel cells. The fault detection and isolation algorithm is based on an artificial neural network classifier, which uses three extracted features as input. Two of the proposed features are based on angles in the impedance spectrum, and are therefore relative to specific points, and shown to be independent of degradation, contrary to other available feature extraction methods in the literature. The experimental data is based on a 35 day experiment, where 2010 unique electrochemical impedance spectroscopy measurements were recorded. The test of the algorithm resulted in a good detectability of the faults, except for high methanol vapour concentration in the anode gas fault, which was found to be difficult to distinguish from a normal operational data. The achieved accuracy for faults related to CO pollution, anode- and cathode stoichiometry is 100 % success rate. Overall global accuracy on the test data is 94.6 %.

Keywords: Fault diagnosis, Classification, Pattern recognition, Fuel Cell, PEM, Electrochemical impedance spectroscopy (EIS)

1. Introduction

In the transition from fossil fuel powered electrical grid to a renewable energy supplied electrical grid, many fluctuating energy sources such as solar and wind have been adopted. Since the renewable energy sources are fluctuating, energy storage technologies are needed, and here hydrogen could play a role, both for transport and stationary applications [1, 2, 3, 4, 5].

Hydrogen storage uses electrolyzers to produces hydrogen from the excess energy in the electrical grid, and when electrical production from renewable energy sources are low the hydrogen is fed into fuel cells, which produce electrical energy. The most common type of fuel cells are proton exchange membrane (PEM) fuel cells, which operate between 60-100 °C with Nafion® as membrane conductor. These fuel cells require high purity of the hydrogen supplied to the fuel cell. An alternative to PEM fuel cells are high temperature proton exchange membrane (HTPEM) fuel cells, which operate between 150-200 °C with phosphoric acid-doped polybenzimidazole (PBI) as membrane conductor [6]. The advantage of HTPEM fuel cells is that they are more tolerant towards impurities in the anode gas, without a gas purification system [7]. The HTPEM fuel cells can thereby be deployed with a methanol reformer system, which is an environmental friendly technology, if the methanol is produced based on renewable hydrogen [8].

Hydrogen storage technologies are expensive and some of the most important factors for commercial success are reliability, cost and durability. The American Department of Energy (DoE) has set ambitious minimum targets for the lifetime of fuel cell applications, meaning 40,000 h for stationary and 5,000 h for automotive, before degrading to 80 % of rated power [9].

One of the ways to improve fuel cell reliability and durability is a well-designed on-line diagnostics scheme, which can detect faults on the fuel cell and with a mitigation strategy impeding fault factors before the fuel cell degradation is accelerated [10, 11].

On-line diagnostic algorithms are usually divided into model based [12] and non-model based [13] methods. Common for these are that they are divided into fuel cell characterization, feature extraction and change detection. For the non-model based methods, the change detection part is often conducted by a machine learning method. Common for many of these diagnostics methods are that the fuel cell characterization often is done by electrochemical impedance spectroscopy (EIS) [12, 13], which has the main advantage that it can be done in-situ at low energy cost [10]. When using EIS as fuel cell characterization technique, the model based methods utilize the parameters of an electrical equivalent circuit (EEC) as features [14, 15, 16]. For the non-model based methods, using EIS as fuel cell characterization method, often uses parts of the impedance spectrum as features for fault detection [17, 18, 19].

The above methods are manly applied on PEM fuel cells and most of them focus on detecting flooding and drying.

*Corresponding author
Email address: chj@et.aau.dk (Christian Jeppesen)
URL: http://et.aau.dk (Christian Jeppesen)

When moving to HTPEM fuel cells the water management issue are no longer present since they are operated above 100 °C, but alternative faults arise when deployed with a hydrocarbon or alcohol-based fuel reformer, such as detecting impurities in the anode gas. Such faults have been addressed in the literature by model based methods using EIS as fuel cell characterization method, and EEC model parameters as features [20, 21]. However, non-model based fault diagnostics method for HTPEM fuel cells have not been investigated yet.

It is a well-established fact in the literature, that the impedance spectrum spread during normal degradation which applies to both the high- and the low-frequency intersect with the real axis. This complies for both PEM fuel cells [22, 23] and HTPEM fuel cells [24]. In the work by Hissel et al. [25] life time EIS data from two different fuel cell stacks, were used to design a fuzzy-clustering algorithm to determine the type of ageing. However, to date there are no fault detecting algorithms for fuel cells, which is robust towards the change in the impedance spectrum due to degradation.

In this work, an impedance data driven non-model based fault detection and isolation (FDI) method is presented. The method is used for the detection of five different faults, which commonly occur on a HTPEM fuel cell methanol reformer systems. To the authors best knowledge a FDI method for HTPEM fuel cells, have not yet been reported in the literature. Furthermore, the described method is independent of the fuel cell degradation, contrary to other available feature extraction methods in the literature.

The paper is structured as follows:
In section 2 the experimental setup and the experimental procedure will be presented. In section 3, the feature extraction and the diagnostic algorithm will be explained. The results will be presented and discussed in section 4. Finally the concluding remarks will be made in section 5.

2. Experimental data foundation

Since the FDI method presented in this work is data-driven, a fuel cell database both in healthy and faulty conditions is necessary. Therefore, tests have been conducted on a short HTPEM fuel cell stack, where real life situations were emulated using a GreenLight Innovation fuel cell test station. The test matrix was based on the operating parameters and conditions of a methanol reformer-HTPEM fuel cell systems, such as the SerEnergy H3-5000 fuel cell system, for healthy and non-healthy operations. The fuel cell stack used for this work is a 10 cell SerEnergy short stack, shown in Figure 1.

As stated in the introduction, EIS will be utilized as fuel cell characterization technique, which is well described in the literature, and is a powerfull characterization technique for fault detection of fuel cells [10, 26]. An electrochemical device such as a fuel cell is a highly non-linear system, and a full mechanistic impedance model based on first principles are very complex. EIS is therefore often used as an empirical linearization of the fuel cell, where a sinusoidal signal is superimposed to the DC value, and by measuring the responding signal, the amplitude ratio and the phase shift can be determined and on that basis the impedance can be calculated. This is often done in galvanostatic mode in fuel cells, where a small AC current perturbation is induced on the DC current load and the voltage response is measured. By sweeping over the desired frequency range, the full impedance spectrum can be determined. The drawback of this method is that the impedance is only valid at one operating point, and therefore, EIS measurements at all the operational points of interest are needed.

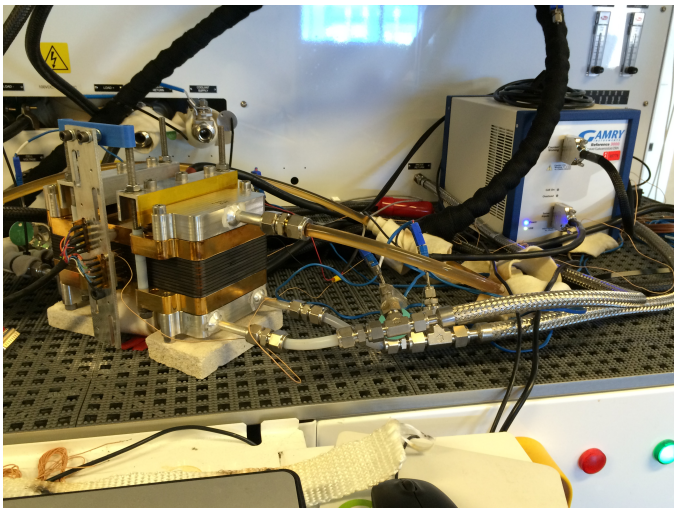

Figure 1: On the right the Gamry Reference 3000 instrument used for impedance measurements is shown. On the left the 10 cell short-stack used for the experimental work is shown. The stack is installed in a GreenLight G200 fuel cell test station, fuel cell faults can be emulated.

Since one of the scopes of this work is designing a FDI algorithm, which is robust toward degradation, the experimental work needs to ensure a large amount of healthy data for determining how the impedance changes during degradation.

2.1. Considered faults

In this work five different conditions identified as abnormal fuel cell operation, are considered as faults (ϕ_1-ϕ_5) and listed in Table 1.

When fuel cell systems are deployed in the field, the cathode oxygen is normally supplied by a fan or a compressor, from the surrounding air. It is desired to be able to detect and isolate faults related to the air delivery system, which can be divided into two different cases:

- ϕ_1 A decrease in cathode stoichiometry (λ_{Air}). This could be due to a faulty fan/compressor or that the deployed systems is at high altitude.
- ϕ_2 An increase in cathode stoichiometry (λ_{Air}). This could be due to a change in fan/compressor characteristics or a software error.

The advantage of HTPEM fuel cells is that they are more tolerant toward impurities in the anode gas, due to the faster kinetics at higher temperatures. HTPEM fuel cells can therefore

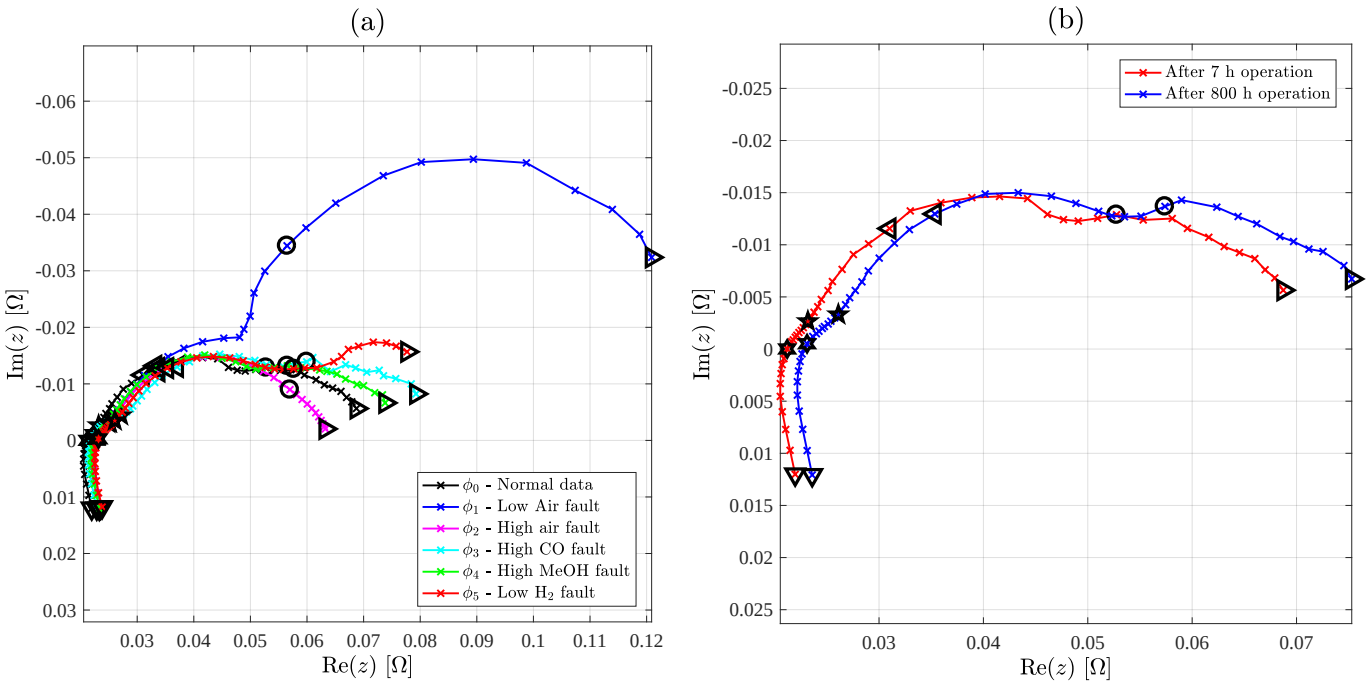

Figure 2: **(a)** Impedance spectra for the 5 different faults considered in this work and normal operation impedance spectra for reference. Impedance spectra measured at 16.5 A. **(b)** Impedance spectra at normal operation conditions, from beginning of experiment and end of experiment. Impedance spectra measured at 16.5 A.

be deployed in combination with a reformer, such as a methanol reformer, without a gas purification system. However, this requires that the reformer is in nominal operation. If the reformer differs from normal operation or the reformer goes into faulty operation, three different effects can occur:

ϕ_3 The anode gas content of carbon monoxide increases from the normal level. This could be due to a change in the temperature profile of the reformer, or a fault on the reformer catalyst.

ϕ_4 Methanol vapour content in the anode gas appears, which could be due to a change in the temperature profile of the reformer, or a fault on the reformer catalyst. Alternatively, it could be due to more methanol delivered by the methanol pump than expected or a fault on the methanol evaporation system.

ϕ_5 A decrease in the anode stoichiometry (λ_{H_2}). This could be due to a decrease in methanol delivered by the methanol pump or due to a fault on the reformer catalyst.

The impedance spectrum for each of the five faults and the normal operation impedance (black), is shown on Figure 2(a). The data shown is from the experiment described in the next section. For the impedance spectrum, the high frequency part (approx. range 1 kHz – 100 Hz) is ascribed to charge transfer in the catalyst layer [27] and the anode activation losses [28, 29]. The intermediate frequency part (approx. range 100 Hz – 5 Hz) of the impedance spectrum is dominated by diffusion losses and the cathode processes and the low frequency part (approx. less than 5 Hz) is attributable to mass transport limitations [26] and oscillation effects in gas composition within the gas flow channels [30, 31].

It can be seen, that the low air fault (ϕ_1), yields the most significant change in the impedance spectrum, caused by an increase in mass transport loss and an increase in diffusion loss on the cathode side. This is more pronounced than the anode side, due to the diluting effect of nitrogen in atmospheric air. This effect is reversed for the high air fault (ϕ_2), where the low frequency arch disappears. For the high CO content fault (ϕ_3), an increase in both high, intermediate and low frequency arches can be observed, due to CO occupying platinum sites. The high frequency arch is increased due to a decrease in anode reaction rate, the intermediate frequency arch is increased, due to a longer path to an available free platinum site and the low frequency arch increases due to the diluting effect yields an increase in gas channel oscillations [32]. For the low hydrogen stoichiometry fault (ϕ_5), the low frequency arch increases, due to mass transport issues and an increase in gas channel oscillations. For the high content of methanol fault (ϕ_4) quite close to the normal operational data (ϕ_0), due to water and methanol vapor mixture has more diluting effect than poisoning effect at these concentrations, which in these experiments causes a slight increase in the intermediate frequency arch due to the diluting effect [33, 34].

2.2. *Experimental procedure*

The experiments for this work is conducted on a 10-cell short stack, based on standard flow plates and MEA's from a SerEnergy S165L stack, with a cell active area of 165 cm^2, nominal power of 41.66 W/cell and maximum rated current density of 0.5 A/cm^2. The stack is installed in a GreenLight fuel cell test

Table 1: Overview of the faults considered. The faults are investigated for the fuel cell current set points 16.5, 24.75, 33, 41.25, 49.5 A with 6 EIS measurements for each fault at each current set point.

Nr.	Fault	Normal	Abnormal
ϕ_1	Low λ_{Air}	2.5 [-]	1.5 [-]
ϕ_2	High λ_{Air}	2.5 [-]	4 [-]
ϕ_3	High CO	0.5 % Vol.	2.5 % Vol.
ϕ_4	High MeOH vapor	0 % Vol.	5 % Vol.
ϕ_5	Low λ_{H_2}	1.4 [-]	1.15 [-]

station, and shown on Figure 1, where the Air, H_2, CO and CO_2 gas flows can be controlled by mass flow controllers. The methanol vapour delivery systems is based on a liquid HPLC pump and a heat exchanger.

Before the experiment, the fuel cell short stack was operated in a break-in procedure as suggested by Vang et al. [35]. The short stack break-in duration was 100 h at 33 A (0.2 A cm^{-2}), with λ_{Air}=4 and λ_{H_2}=2.

The experiment duration is 35 days, where each day is structured as shown on Figure 3(a). During the first 6 h and aprox. the last 8 h of each day, the stack is operated at 82.5 A, which corresponds to 0.5 Acm^{-2}. After the first 6 h of operation the fuel cell characterization is scheduled at 16.5 A (0.1 Acm^{-2}), 24.75 A (0.15 Acm^{-2}), 33 A (0.2 Acm^{-2}), 41.25 A (0.25 Acm^{-2}) and 49.5 A (0.3 Acm^{-2}). 12 EIS measurements were conducted at each current set point. This procedure is repeated every day, except for day 14, 21, 28 and 35, where a faulty condition is introduced. The same current set points are repeated for each faulty operation, with 6 EIS measurements at each current set point. An overview of the number of EIS measurements is given in Table 2.

On day 14 the low air stoichiometry, fault (ϕ_1) and high air stoichiometry, fault (ϕ_2) were induced; on day 21 high content of CO was introduced in the anode gas, fault (ϕ_3); on day 28 high content of MeOH vapour was introduced in the anode gas, fault (ϕ_4) and on day 35 the low anode stoichiometry, fault (ϕ_5) is induced.

The overview of the fuel cell stack voltage and current for the entire experiment is given in Figure 3(b).

2.2.1. Gas composition

The anode gas composition is based on experience with a H3-5000 SerEnergy methanol reformer. Hydrogen fraction is kept constant at 75 % by volume, and for normal days the CO content is kept at 0.5 % by volume. CO_2 is used as a fill gas, meaning that at normal days the CO_2 fraction is kept at 24.5 % by volume of the total anode gas flow, and at abnormal days the CO_2 fraction is kept lower. The stoichiometric ratios are kept at λ_{Air}=2.5 and λ_{H_2}=1.4 during the experiment, except for day 14 and day 35, where they are changed accordingly to Table 1.

2.2.2. Gas humidification

The anode gas is humidified by mean of a bubbler, with a dew point temperature of 49 °C. This corresponds the anode

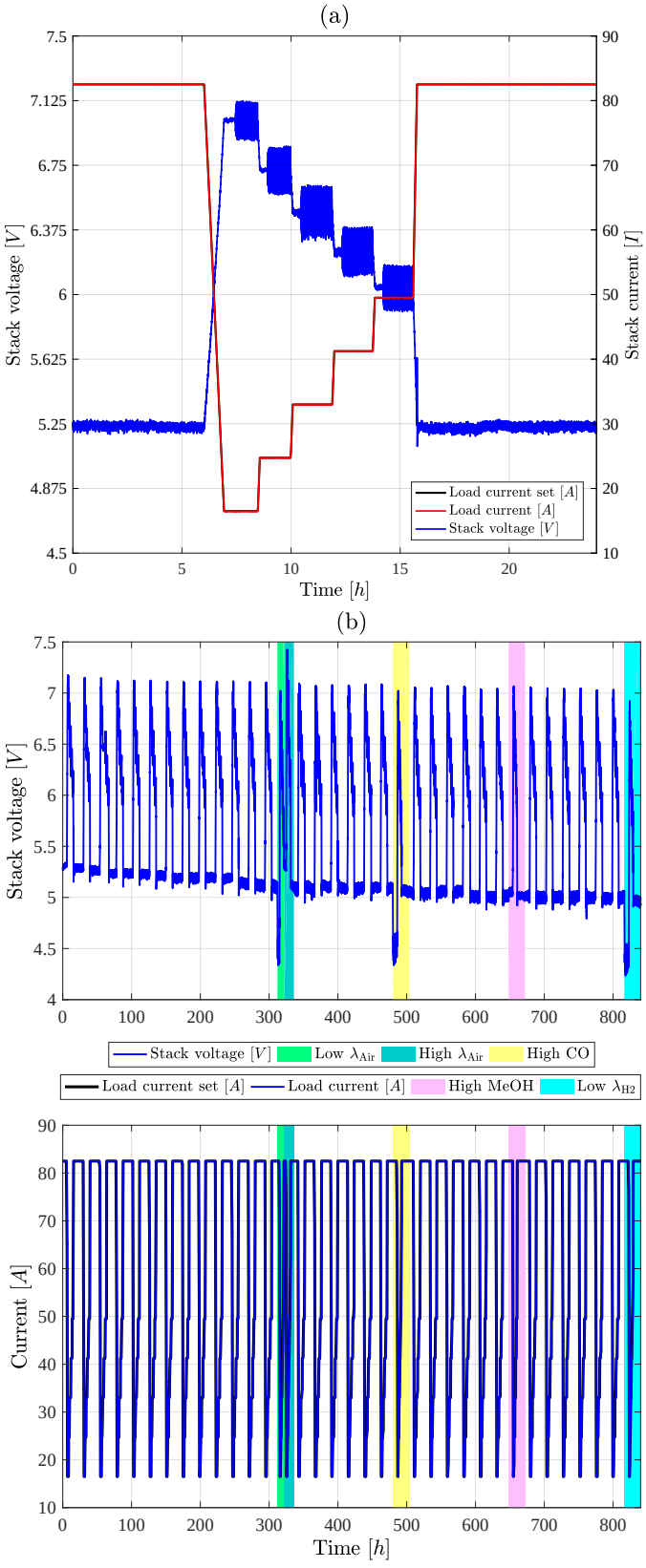

Figure 3: **(a)** Stack voltage and current during a day with normal operating conditions. During the characterization 12 EIS measurements is acquired at each current set point. **(b)** Fuel cell stack voltage and current during the entire 810 h experiment, corresponding to 35 days of operation.

Table 2: Overview of the set points during the fuel cell characterization experiment.

	No. of EIS
Nr. at each normal current set point	12
Nr. at each abnormal current set point	6
Total at Normal day	60
Total at Abnormal day	30
Total experiment	2010

gas water content, for the output gas of a methanol steam reformer operating with a fuel steam to carbon ration of 1.5. A mass flow controller supplies the cathode gas, from oil free air compressor.

2.2.3. Temperature

The short stack of subject in this work is oil heated and cooled by an external cooling cart using Paratherm oil, in a closed circuit. The temperature controller is set to keep a fuel cell output temperature of 167 °C throughout the entire experiment. When changing current set point, a current ramp of 0.05 As^{-1} is applied to ensure minimum temperature variation. Furthermore, a 20 min delay without any temperature deviations of more than 0.5 °C is performed, before any EIS measurement is conducted.

2.2.4. EIS measurements

For EIS measurements a Gamry Reference 3000, running in galvanostatic mode is utilized. The AC current amplitude is set to 7.5 % of current DC value, as recommended by Dale et al. [36], however, with a maximum of ±3 A due to instrumental limitation. The starting frequency is 10 kHz and the end frequency is 0.1 Hz with 10 points pr. decade, divided into logarithmic intervals. In Table 2 the number of EIS measurements at each current set point and at each day are listed.

3. FDI Algorithm

As seen in Figure 2(b), the impedance spectrum changes due to degradation. The impedance spectrum spreads and moves to the right during degradation, which manifest itself by an increase in the series resistance (the first intersect with the real axis), and more significantly expressed by an increasing real part of the low frequency part of the spectrum. The observed ageing mode is common for high temperature PEM fuel cells [37, 38, 39]. Thus, it is evident that an impedance based FDI algorithm for fuel cell applications needs to be robust towards degradation.

In this work, a feedforward artificial neural network (ANN) classifier fault detection and isolation (FDI) methodology is proposed, for detecting the faults listed in Table 1. The principle of the methodology is illustrated in Figure 4, where the four different steps are listed. This is a supervised machine learning approach, and therefore the 2010 EIS measurements, from the experiment described in section 2.2, needs to be labeled with the 6 different cases (ϕ_0-ϕ_5), prior to the training, validation and testing of the ANN classifier.

The proposed FDI methodology initially takes a real time EIS measurement from a deployed fuel cell system, runs the acquired impedance spectrum through a pre-processing layer, which will be described in section 3.1. Hereafter three selected features will be calculated based on section 3.2, which are used as input to the ANN classifier algorithm. The ANN classifier algorithm which is trained is explained in section 3.3.

3.1. Data pre-processing

After the EIS measurement is acquired, a pre-processing step of the methodology is applied. The purpose of this step is to prepare the impedance spectrum for the feature calculation. Some of the EIS measurements, especially at higher currents are slightly noisy, for the low frequencies. The primarily reason for this, is the ±3 A current limit of the Gamry galvanostat used for the experimental characterization. This makes the relative AC current amplitude smaller compared to the DC component of the fuel cell current, and thereby decreasing the signal to noise ratio. The impedance spectrum is therefore filtered, for noise rejection.

The filter used in the pre-processing step is a zero phase butterworth filter, by filtering the impedance spectrum in both forward and reverse direction [40], going from high to low and again back to high frequency. Two examples can be seen in Figure 5(a), where a low noise spectrum can be seen (red) and a high noise spectrum (magenta). For the low noise spectrum it can be observed that the phase between the unfiltered and the filtered data is low, and for the high noise spectrum it can be noted that the filter rejects the noisy measurement points.

3.2. Feature extraction/selection

For dimensional reduction of the measurements space, for FDI algorithms for fuel cell applications using EIS as characterization, there are in general two different approaches, feature extraction or feature selection.

Feature selection is preformed, by directly choosing k of the d dimensions which yield the most information needed for the fault classification, where d is the dimension of the measurements space [18, 41]. Alternatively, k features can be calculated based on the measurement space, as a feature extraction. Some of the most common dimensional reduction methods described in machine learning literature are statistically based methods such as principal component analysis and linear discriminant analysis [13, 41]. Alternatively, feature extraction can be performed by fitting an electrical equivalent circuit to the impedance spectrum, and using the parameters as features [20, 42], mathematically representing the impedance spectrum by more generic model, or extracting features which are based on knowledge of the fault nature.

This work will be based on simple knowledge based feature extraction. In Figure 5(b), a common impedance spectrum is illustrated, with the four (a-d) knowledge based features found in the literature. The four features are listed here:

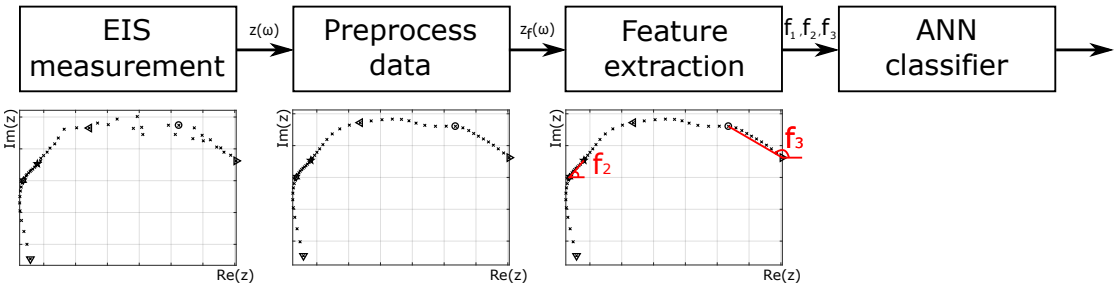

Figure 4: Flow chart of the proposed artificial neural network fault detection and isolation methodology.

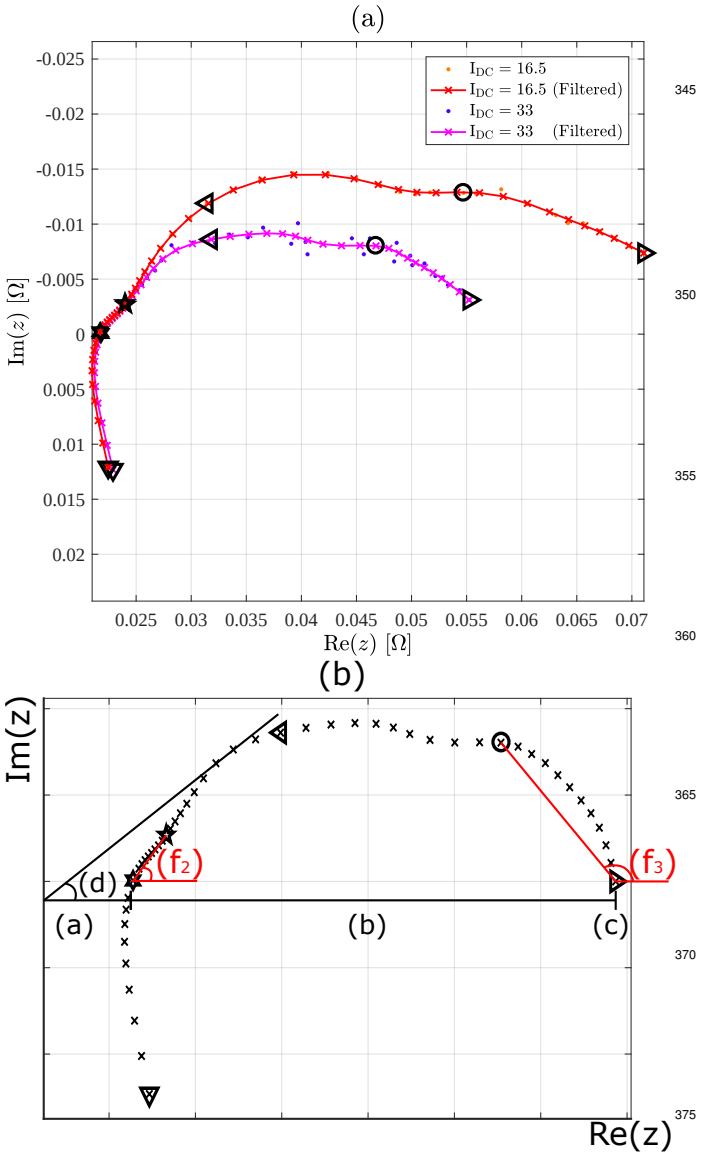

Figure 5: **(a)** Impedance spectra for 16.5 and 33 A at day 2, before and after preprocessing. **(b)** Features found in the literature ((a)-(d)) and the two features (f_2 , f_3) used for this work.

(a) The internal series resistance, often extracted as the value of the first intersect with the real axis [17]

(b) The difference between the internal resistance and the real part of the second intersect with the real axis, or put differently, the span of the impedance spectrum [19, 25].

(c) The second intersect with the real axis, sometimes denoted as the polarizing resistance or just the maximum amplitude of the impedance spectrum [19, 43].

(d) The maximum angle of the impedance spectrum [17, 43] or the frequency at the maximum angle [19].

The features (a-d), which are shown in Figure 5 and listed above, are often used for detecting flooding and drying of low temperature PEM fuel cells [17, 19, 43]. The faults considered in this work are listed in Table 1, and are for HTPEM applications. Some of the features above like the series resistance are therefore not useful for this algorithm. In addition, it can be seen that some extracted features change with degradation. This is illustrated in Figure 6(a), where 4 different extracted features are plotted with respect to degradation. In Figure 6(a), the top left is the internal series resistance (represented as the high frequency intercept) plotted with respect to fuel cell operational time, and the top right is the real value of the 0.1 Hz impedance point plotted. In Figure 6(a), the two bottom figures shows how the internal magnitude of the spectrum changes relatively to the operational time. It can be seen that the features shown in Figure 6(a), change with the operational time and thereby the degradation. It is not desirable to use features, that change with time, since the design of thresholds become difficult. When features change with time, the fault detection becomes more prone to false alarm or false detection.

A self-cognizant diagnostic methodology could solve this problem, by adapting to the change in features as result of degradation. Alternatively, a set of features that are constant for healthy operation and independent of degradation could be chosen, if possible.

Different methods to extract features from the impedance spectrum have been analyzed in this work, as shown in Figure 6(a). Two features extraction methods were found to be independent of degradation and suitable for detecting the faults listed in Table 1, and are chosen based on user experience. The two suggested feature extraction methods

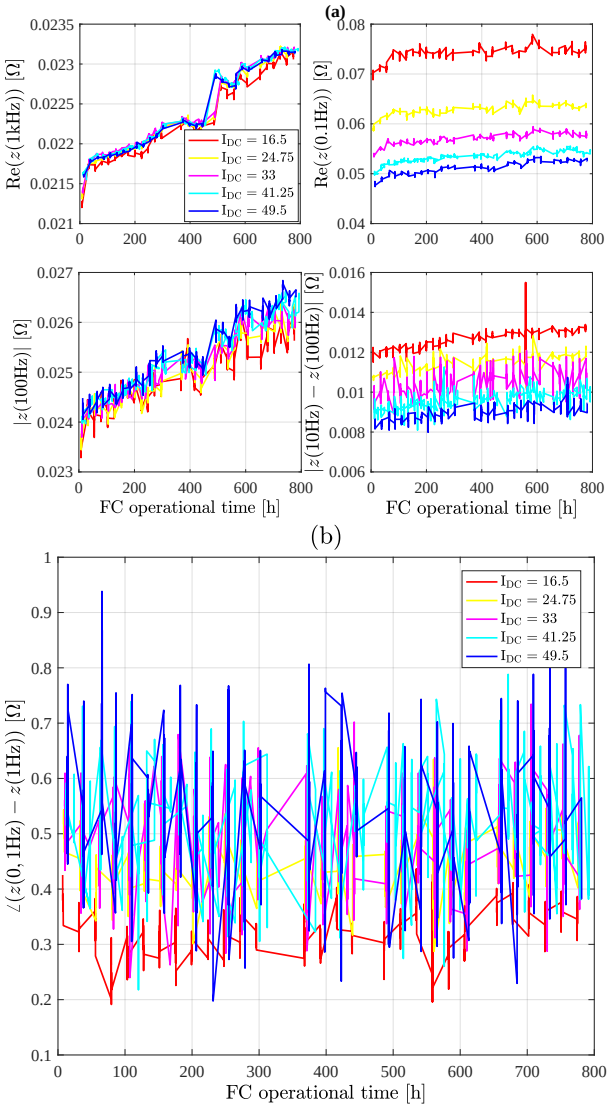

Figure 6: **(a)** Selection of features that change with degradation. All data for normal operation. **(b)** The feature f_3 for normal operational data, as function of the fuel cell operational time.

Table 3: Description of the three features, which is used as input to the ANN classifier.

Feature No.	**Description**
f_1	DC component of fuel cell current
f_2	$\angle(z(100\text{Hz}) - z(1\text{kHz}))$
f_3	$\angle(z(0.1\text{Hz}) - z(1\text{Hz}))$

Table 4: Based on empirical analysis, how the features f_2 and f_3 changes, for the faults ϕ_1 - ϕ_5.

	ϕ_0	ϕ_1	ϕ_2	ϕ_3	ϕ_4	ϕ_5
f_2	-	-	-	↑	↓	-
f_3	-	↓	↑	-	-	↓

are listed in Table 3 as f_2 and f_3 and in combined with the DC component of the current. The features f_2 and f_3 are the angles between the frequencies decades 1 kHz to 100 Hz (f_1) and 1 Hz to 0.1 Hz (f_2). Since the features are angles of the spectrum, they are relative and do not change with respect to degradation, as illustrated for feature f_3 in Figure 6(b). In Figure 6(b) it can also be seen that the feature f_3 is dependent on the fuel cell current, and for this reason, the DC component of fuel cell current is chosen as the third feature (f_1).

The behavior of the features f_2 and f_3 under normal and faulty conditions, is shown in Figure 7(a), for the entire data set at 16.5 A. As stated in Table 4, it can be seen that faults ϕ_3 and ϕ_4 are correlated with feature f_2 and the faults ϕ_1, ϕ_2 and ϕ_5 are correlated with feature f_3. The faults ϕ_1, ϕ_2 and ϕ_5 are related to the delivery of fuel and oxidant, and is therefore mainly linked to mass transport effects (given in the range of f_3). The faults ϕ_3 and ϕ_4 are related to the anode reaction, and the effect is therefore seen in the high and intermediate frequency part, which affects the angle between the 1 kHz – 100 Hz, and thereby the feature f_2. Furthermore, it can be observed that a high methanol vapour in the anode gas (ϕ_4), is quite close to the normal operation data set. Thus, it is expected that that fault is harder to detect and isolate.

In Figure 7(b), the entire feature space with the entire data set is plotted. Here, it can be seen that the value of the features f_2 and f_3 changes with f_1, and therefore, it is necessary to include the DC component of the fuel cell current as a feature.

3.3. ANN classifier and the training

As fault detection and isolation classifier, a feed forward neural network is trained for the task. In Figure 8, an overview of the offline training is illustrated. Firstly, the experimental data from the experiment described in section 2.2, is labeled with a fault identifier (ϕ_0-ϕ_5) and the features (f_1 - f_3) are calculated for each of the 2010 EIS measurements. Next, the data set is divided into training data, validation data and test data. The test data is manually selected for ensuring that each fault case is equally represented. For each day at non-healthy operation two EIS measurements are reserved for testing at each current set point, and for each day at healthy operation one EIS measurement is reserved for testing at each current set point. The

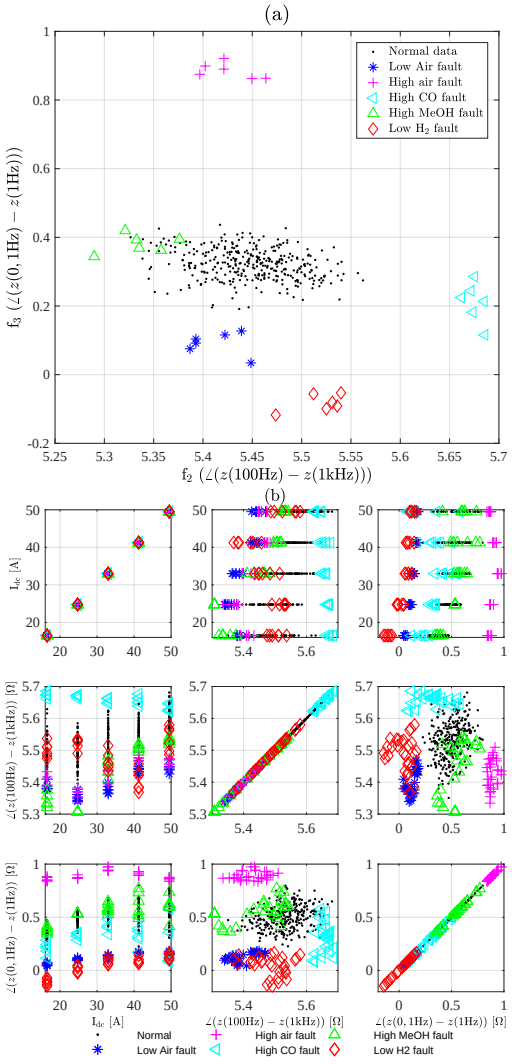

Figure 7: **(a)** Feature space $\{f_2\ ,\ f_3\}$ for the entire experiment at 16.5 A. **(b)** Feature space $\{f_1\ ,\ f_2\ ,\ f_3\}$ for the entire experiment.

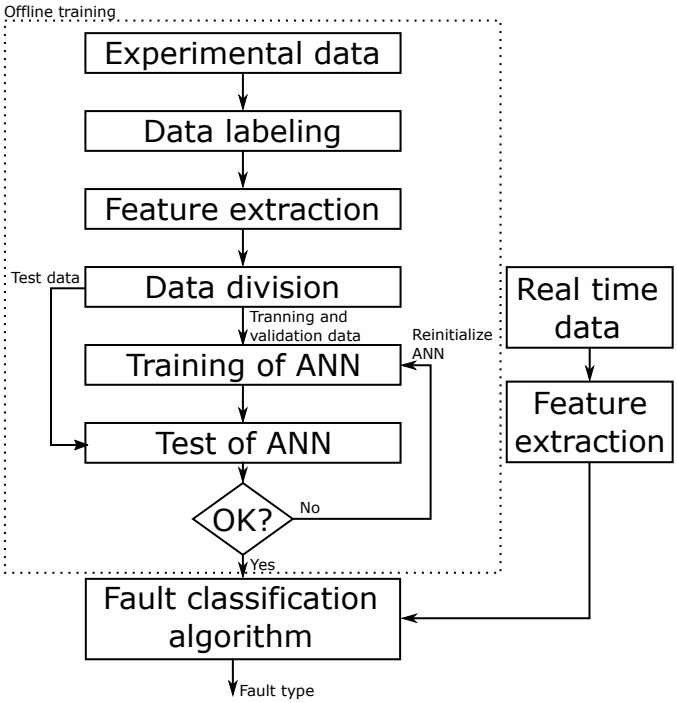

Figure 8: Offline procedure for the training of artificial neural network in the dashed square. For the online procedure, an EIS measurement is acquired, the feature extraction is calculated, and the features is used for input to the artificial neural network.

Table 5: In percentage, how the entire dataset (2010 EIS measurements) is divided in the training, validation and test data subsets. Test dataset in selected, and the remaining data in randomly divided into training and validation data subsets.

	% of data
Training data	76 %
Validation data	14 %
Test data	10 %

remaining data set is split randomly with 85 % for training and 15 % for validation. An overview of the allocation of the overall data is given in Table 5. Devoting 76 % of the dataset to training is similar to other studies described in the literature [17].

The training data is used in the training process of the ANN classifier, the validation data is used as a stop criteria for the training algorithm and the test data is used for human expert approval of the ANN classifier performance.

The feed forward ANN consists of one hidden layer with 10 neurons and with a tansig transfer function and an output layer with one outlet for each of the fault cases, with a soft-max transfer function. No normalization of any of the inputs is performed.

As training the scaled conjugate gradient optimization algorithm is utilized. As stop criteria for the training there are three options; 10 number of validation checks, where the ANN performance has not increased, the gradient becomes less than 10^{-6} or the performance becomes 0, where the performance is calculated as the Cross-Entropy.

Table 6: The result of the test data, listed in a confusion matrix. The results are listed in %. Global accuracy is 94.6 %.

ANN output class \ Target class	ϕ_0	ϕ_1	ϕ_2	ϕ_3	ϕ_4	ϕ_5
ϕ_0	98	0	0	0	70	0
ϕ_1	0	100	0	0	0	0
ϕ_2	0	0	100	0	0	0
ϕ_3	0	0	0	100	0	0
ϕ_4	2	0	0	0	30	0
ϕ_5	0	0	0	0	0	100

4. Results and discussion

4.1. Training results accuracy and performance evaluation

The proposed ANN classifier methodology presented in the previous section, in combination with the proposed features, has in general proven to be well suited for fault detection and isolation, of the five faults (ϕ_1-ϕ_5) listed in Table 1.

The results of the test data (10% of the entire dataset) are listed in a confusion matrix between the ANN output and the actual target class, in Table 6. It can be seen that the faults ϕ_1, ϕ_2 and ϕ_3 and ϕ_5 have 100 % success rate. As it can be seen in Table 6, the ANN classifier has problems distinguishing between high methanol content fault and normal operation data. This is supported by Figure 2(a), where it can be seen that the impedance spectrum of high methanol vapour concentration in the anode gas fault (ϕ_4), is quite close to the impedance spectrum of the normal operation data (ϕ_0).

To improve detectability of fault ϕ_4, the methanol concentration could be increased. However, a methanol vapour concentration of 5% is considered a well-established fault and would not be considered as early detection. Furthermore, it is expected that a higher than 5% methanol vapour concentration would yield an impedance signature comparable to the high CO concentration fault (ϕ_3), and therefore, a higher than 5% methanol vapour concentration fault would only move the problem to distinguishing between high CO and high methanol concentrations.

The global accuracy of the test data classification using the proposed methodology is 94.6 %. This is good in line with previously reported values in the literature, for LTPEM fuel cell FDI. Hissel et al. [25] reported a 89 % accuracy and Zheng et al. [19] reported a 100 % accuracy, both using a Fuzzy Clustering Algorithm. Onanena et al. [17] did a comparison of k-nearest neighbor and linear discriminant analysis with two different ways of feature extraction, which yielded a 93.9 % - 99.6 % accuracy for different methods.

4.2. Discussion

One of the benefits to this methodology, compared to using the parameters of an equivalent electrical circuit, is that it is not necessary to acquire the entire spectrum, but only impedance at four frequencies. To acquire an incomplete impedance spectrum is less time consuming than acquiring the full spectrum, which is an advantage since there are less risk that the fuel cell moves away from steady state operation. In this work, the entire impedance spectrum was acquired, and therefore, if only the relevant frequencies were measured, the pre-processing part of the methodology would need to be changed, e.g. by calculating the average of the impedance at the neighboring frequency points.

One of the major issues with EIS as reported in literature is complex data processing and time consuming process. Here in the present work the frequency domain is reduced and hence the data processing and the measurement time is relatively smaller. The accuracy level of the measurements in separating out the different faulty conditions are quite high which makes the process more promising and efficient. The FDI methodology from the present study could be easily implemented in the existing fuel cell system with minor modification provided the training is carried out offline. The study takes into account the degradation of the cell which makes the algorithm robust and minimal human interference as required in some others FDI methods proposed in the literature's.

This work builds on a data driven method, and there is no knowledge of how the methodology would perform if utilized on a different stack from another production batch. Therefore, for deploying this methodology in the field, a larger database with impedance data from different production batches is needed, since there is no information of the impedance variance from stack to stack in the literature.

Furthermore, this analysis was carried out on a 10 cell short stack, but normally a fuel cell of this type is deployed in the field in a 60 or 120 cells configuration. The experimental procedure would therefore need to be reinitialized for a full-size stack. Moreover, the impedance spectrum of full-size HTPEM stack is not reported in literature, for the faults considered in this work. This could be subject of future studies.

The experiments for this work were performed on laboratory scale, with a Gamry galvanostat for impedance measurements. This implementation is quite expensive, and is therefore not suited for in-field implementation. However, some EU projects work on implementing the EIS characterization method on the onboard DC/DC converter (D-code project Grant: 256673). This requires great attention to the bandwidth of the DC/DC converter and requirements to the onboard computer. In this work all data processing was done offline, which would not be the case for a system in the field.

Based on this work, there is no evidence how the algorithm will perform for faults at intermediate fault amplitude. For-example, a larger concentration of CO (ϕ_3) could resemble the low anode stoichiometry fault (ϕ_5) or a lower concentration of CO could resemble the high methanol vapour concentration fault (ϕ_4). This could be subject of future studies.

5. Conclusions

In this work a methodology for fault detection and isolation of low and high cathode stoichiometry, high CO concentration

in the anode gas, high methanol vapour concentration in the anode gas and low anode stoichiometry was proposed, for high temperature PEM fuel cells. The fault detection and isolation methodology is data driven based on the impedance spectrum.

The fault detection and isolation is divided into 4 steps; acquiring of EIS measurement, pre-processing of data, feature extraction and artificial neural network classification of fault class. The pre-processing of the impedance spectrum is conducted by a zero phase Butterworth filter, which is used to remove outliers. The extracted features used in this work are the DC component of the fuel cell current, and two angles between the impedance at 100 Hz and 1 kHz and between 0.1 Hz and 1 Hz.

A broad selection of features is analyzed with respect to degradation, and it is found that the selected features do not depend on the fuel cell degradation. Therefore, unlike many of the selection feature extraction methods commonly found in the literature, there is no need to retrain the artificial neural network classifier, during the life time of the fuel cell stack.

The experimental data foundation is based on a 35 day experiment, where the first week is fault free and hereafter a new fault is introduced on the last day of the week, for the remainder 3 weeks. This results in 2010 unique EIS measurements under the influence of degradation.

The proposed fault detection and isolation methodology is based on an artificial neural network classifier, which is trained on 76 % of the entire data-set and validated on 14 % of the data-set. 10 % of the data-set is used for testing the algorithm.

Overall global accuracy on the test data is 94.6 %, which is considered a good result, and it can be concluded that the artificial neural network together with the suggested features, is feasible for fault detection and isolation. The achieved accuracy for faults related to CO pollution, anode- and cathode stoichiometry is 100 % success rate. It can be concluded that the proposed algorithm has difficulties distinguishing between the high methanol vapour concentration in the anode gas fault and normal operational data.

Acknowledgments

The work was supported by Innovation Fund Denmark in the frame of the 4M Centre. The authors would also like to acknowledge SerEnergy A/S for supplying the short-stack for experimental work.

References

[1] M. Becherif, H. S. Ramadan, K. Cabaret, F. Picard, N. Simoncini, O. Bethoux, Hydrogen Energy Storage: New Techno-Economic Emergence Solution Analysis, Energy Procedia 74 (0) (2015) 371–380. doi:10.1016/j.egypro.2015.07.629.

[2] J. Andrews, B. Shabani, Re-envisioning the role of hydrogen in a sustainable energy economy, International Journal of Hydrogen Energy 37 (2) (2012) 1184–1203. doi:10.1016/j.ijhydene.2011.09.137.

[3] G. Gahleitner, Hydrogen from renewable electricity: An international review of power-to-gas pilot plants for stationary applications, International Journal of Hydrogen Energy 38 (5) (2013) 2039–2061. doi:10.1016/j.ijhydene.2012.12.010.

[4] G. Krajačić, R. Martins, A. Busuttil, N. Duić, M. da Graça Carvalho, Hydrogen as an energy vector in the islands' energy supply, International Journal of Hydrogen Energy 33 (4) (2008) 1091–1103. doi:10.1016/j.ijhydene.2007.12.025.

[5] D. Teichmann, W. Arlt, P. Wasserscheid, Liquid Organic Hydrogen Carriers as an efficient vector for the transport and storage of renewable energy, International Journal of Hydrogen Energy 37 (23) (2012) 18118–18132. doi:10.1016/j.ijhydene.2012.08.066.

[6] Q. Li, R. He, J. Jensen, N. Bjerrum, Approaches and recent development of polymer electrolyte membranes for fuel cells operating above 100 C, Chemistry of materials (2003) 4896–4915doi:10.1021/cm0310519.

[7] S. S. Araya, F. Zhou, V. Liso, S. L. Sahlin, J. R. Vang, S. Thomas, X. Gao, C. Jeppesen, S. K. Kær, A comprehensive review of PBI-based high temperature PEM fuel cells, International Journal of Hydrogen Energy 41 (46) (2016) 21310–21344. doi:10.1016/j.ijhydene.2016.09.024.

[8] G. A. Olah, A. Goeppert, G. K. S. Prakash, Chemical recycling of carbon dioxide to methanol and dimethyl ether: From greenhouse gas to renewable, environmentally carbon neutral fuels and synthetic hydrocarbons, Journal of Organic Chemistry 74 (2) (2009) 487–498. doi:10.1021/jo801260f.

[9] U.S. DOE., The Fuel Cell Technologies Office Multi-Year Research, Development, and Demonstration Plan, Tech. rep., U.S. Department of Energy (2016).
URL https://energy.gov/eere/fuelcells/fuel-cells

[10] D. Hissel, M. Pera, Diagnostic & health management of fuel cell systems: Issues and solutions, Annual Reviews in Control 42 (2016) 201–211. doi:10.1016/j.arcontrol.2016.09.005.

[11] C. Cadet, S. Jemeï, F. Druart, D. Hissel, Diagnostic tools for PEMFCs: from conception to implementation, International Journal of Hydrogen Energy 39 (20) (2014) 10613–10626. doi:http://dx.doi.org/10.1016/j.ijhydene.2014.04.163.

[12] R. Petrone, Z. Zheng, D. Hissel, M. C. Péra, C. Pianese, M. Sorrentino, M. Becherif, N. Yousfi-Steiner, A review on model-based diagnosis methodologies for PEMFCs, International Journal of Hydrogen Energy 38 (17) (2013) 7077–7091. doi:10.1016/j.ijhydene.2013.03.106.

[13] Z. Zheng, R. Petrone, M. C. Péra, D. Hissel, M. Becherif, C. Pianese, N. Yousfi Steiner, M. Sorrentino, A review on non-model based diagnosis methodologies for PEM fuel cell stacks and systems, International Journal of Hydrogen Energy 38 (21) (2013) 8914–8926. doi:10.1016/j.ijhydene.2013.04.007.

[14] P. Polverino, C. Pianese, M. Sorrentino, D. Marra, Model-based development of a fault signature matrix to improve solid oxide fuel cell systems on-site diagnosis, Journal of Power Sources 280 (2015) 320–338. doi:10.1016/j.jpowsour.2015.01.037.

[15] T. Génevé, J. Régnier, C. Turpin, Fuel cell flooding diagnosis based on time-constant spectrum analysis, International Journal of Hydrogen Energy 41 (1) (2016) 516–523. doi:10.1016/j.ijhydene.2015.10.089.

[16] G. Mousa, J. Devaal, F. Golnaraghi, Diagnosis of hydrogen crossover and emission in proton exchange membrane fuel cells, International Journal of Hydrogen Energy 39 (35) (2014) 20116–20126. doi:10.1016/j.ijhydene.2014.09.116.

[17] P. A. R. Onanena, L Oukhellou, E Côme, D Candusso, D Hissel, Fault-diagnosis of PEM fuel cells using electrochemical spectroscopy impedance, Power Plants and Power Systems Control (2012) 651–656doi:10.3182/20120902-4-FR-2032.00114.

[18] A. Debenjak, M. Gašperin, B. Pregelj, M. Atanasijević-Kunc, J. Petrovčič, V. Jovan, Detection of flooding and drying inside a PEM fuel cell stack, Strojniski Vestnik/Journal of Mechanical Engineering 59 (1) (2013) 56–64. doi:10.5545/sv-jme.2012.640.

[19] Z. Zheng, M. C. Péra, D. Hissel, M. Becherif, K. S. Agbli, Y. Li, A double-fuzzy diagnostic methodology dedicated to online fault diagnosis of proton exchange membrane fuel cell stacks, Journal of Power Sources 271 (2014) 570–581. doi:10.1016/j.jpowsour.2014.07.157.

[20] C. Jeppesen, M. Blanke, F. Zhou, S. J. Andreasen, Diagnosis of CO Pollution in HTPEM Fuel Cell using Statistical Change Detection, IFAC-PapersOnLine 48 (2015) 547–553. doi:10.1016/j.ifacol.2015.09.583.

[21] C. de Beer, P. Barendse, P. Pillay, B. Bullecks, R. Rengaswamy, Electrical circuit analysis of CO poisoning in high temperature PEM fuel

cells for rapid fault diagnostics, 2013 IEEE Energy Conversion Congress and Exposition 51 (1) (2013) 4623–4630. doi:10.1109/ECCE.2013.6647320.

[22] R. Chattot, S. Escribano, Ageing studies of a PEM Fuel Cell stack developed for reformate fuel operation in μCHP units: Development of an accelerated degradation procedure, International Journal of Hydrogen Energy 0 (2014) 1–8. doi:10.1016/j.ijhydene.2015.01.066.

[23] R. Onanena, L. Oukhellou, D. Candusso, F. Harel, D. Hissel, P. Aknin, Fuel cells static and dynamic characterizations as tools for the estimation of their ageing time, International Journal of Hydrogen Energy 36 (2) (2011) 1730–1739. doi:10.1016/j.ijhydene.2010.10.064.

[24] P. Moçotéguy, B. Ludwig, J. Scholta, R. Barrera, S. Ginocchio, Long term testing in continuous mode of HT-PEMFC based H3PO 4/PBI celtec-PMEAs for μ-CHP applications, Fuel Cells 9 (4) (2009) 325–348. doi:10.1002/fuce.200800134.

[25] D. Hissel, D. Candusso, F. Harel, Fuzzy-clustering durability diagnosis of polymer electrolyte fuel cells dedicated to transportation applications, IEEE Transactions on Vehicular Technology 56 (5 I) (2007) 2414–2420. doi:10.1109/TVT.2007.898389.

[26] S. M. Rezaei Niya, M. Hoorfar, Study of proton exchange membrane fuel cells using electrochemical impedance spectroscopy technique - A review, Journal of Power Sources 240 (2013) 281–293. doi:10.1016/j.jpowsour.2013.04.011.

[27] T. E. Springer, T. A. Zawodzinski, M. S. Wilson, S. Gottesfeld, Characterization of Polymer Electrolyte Fuel Cells Using AC Impedance Spectroscopy, Journal of the Electrochemical Society 143 (2) (1996) 587–599. doi:10.1149/1.1836485.

[28] C. Y. Chen, W. H. Lai, Effects of temperature and humidity on the cell performance and resistance of a phosphoric acid doped polybenzimidazole fuel cell, Journal of Power Sources 195 (21) (2010) 7152–7159. doi:10.1016/j.jpowsour.2010.05.057.

[29] S. J. Andreasen, S. K. Kær, Dynamic Model of the High Temperature Proton Exchange Membrane Fuel Cell Stack Temperature, Journal of Fuel Cell Science and Technology 6 (4) (2009) 41006. doi:10.1115/1.3081461.

[30] I. a. Schneider, S. a. Freunberger, D. Kramer, A. Wokaun, G. G. Scherer, Oscillations in Gas Channels - Part I. The Forgotten Player in Impedance Spectroscopy in PEFCs, Journal of The Electrochemical Society 154 (4) (2007) B383—-B388. doi:10.1149/1.2435706.

[31] I. a. Schneider, S. a. Freunberger, D. Kramer, A. Wokaun, G. G. Scherer, Oscillations in Gas Channels - Part II. Unraveling the Characteristics of the Low Frequency Loop in Air-Fed PEFC Impedance Spectra, Journal of The Electrochemical Society 154 (4) (2007) B770—-B782. doi:10.1149/1.2742291.

[32] S. J. Andreasen, J. R. Vang, S. K. Kær, High temperature PEM fuel cell performance characterisation with CO and CO2 using electrochemical impedance spectroscopy, International Journal of Hydrogen Energy 36 (16) (2011) 9815–9830. doi:10.1016/j.ijhydene.2011.04.076.

[33] S. Simon Araya, I. F. Grigoras, F. Zhou, S. J. Andreasen, S. K. Kær, Performance and endurance of a high temperature PEM fuel cell operated on methanol reformate, International Journal of Hydrogen Energy 39 (32) (2014) 18343–18350. doi:10.1016/j.ijhydene.2014.09.007.

[34] S. Thomas, J. R. Vang, S. S. Araya, S. K. Kær, Experimental study to distinguish the effects of methanol slip and water vapour on a high temperature PEM fuel cell at different operating conditions, Applied Energy (2016) –doi:http://dx.doi.org/10.1016/j.apenergy.2016.11.063.

[35] J. R. Vang, S. J. Andreasen, S. S. Araya, S. K. Kær, Comparative study of the break in process of post doped and sol-gel high temperature proton exchange membrane fuel cells, International Journal of Hydrogen Energy 39 (27) (2014) 14959–14968. doi:10.1016/j.ijhydene.2014.07.017.

[36] N. V. Dale, M. D. Mann, H. Salehfar, A. M. Dhirde, T.-H. Han, ac Impedance Study of a Proton Exchange Membrane Fuel Cell Stack Under Various Loading Conditions, Journal of Fuel Cell Science and Technology 7 (3) (2010) 031010. doi:10.1115/1.3207871.

[37] F. Zhou, S. Simon Araya, I. Florentina Grigoras, S. Juhl Andreasen, S. Knudsen Kær, Performance Degradation Tests of Phosphoric Acid Doped Polybenzimidazole Membrane Based High Temperature Polymer Electrolyte Membrane Fuel Cells, Journal of Fuel Cell Science and Technology 12 (2) (2015) 21002. doi:10.1115/1.4029081.

[38] F. Javier Pinar, M. Rastedt, N. Pilinski, P. Wagner, Effect of idling temperature on high temperature polymer electrolyte membrane fuel cell degradation under simulated start/stop cycling conditions, International Journal of Hydrogen Energy 41 (42) (2016) 19463–19474. doi:10.1016/j.ijhydene.2016.05.091.

[39] S. Lang, T. J. Kazdal, F. Kühl, M. J. Hampe, Experimental investigation and numerical simulation of the electrolyte loss in a HT-PEM fuel cell, International Journal of Hydrogen Energy 40 (2) (2015) 1163–1172. doi:10.1016/j.ijhydene.2014.11.041.

[40] A. V. Oppenheim, W. S. Ronald, J. R. Buck, Discrete-Time Signal Processing, 2nd Edition, Prentice Hall, 1999.

[41] E. Alpaydin, Introduction to Machine Learning, 2nd Edition, The MIT Press, 2010.

[42] N. Fouquet, C. Doulet, C. Nouillant, G. Dauphin-Tanguy, B. Ould-Bouamama, Model based PEM fuel cell state-of-health monitoring via ac impedance measurements, Journal of Power Sources 159 (2) (2006) 905–913. doi:10.1016/j.jpowsour.2005.11.035.

[43] Z. Zheng, R. Petrone, M. C. Pera, D. Hissel, M. Becherif, C. Pianese, Diagnosis of a commercial PEM fuel cell stack via incomplete spectra and fuzzy clustering, IECON Proceedings (Industrial Electronics Conference) (2013) 1595–1600doi:10.1109/IECON.2013.6699371.